# The behaviour of charged particles (ions) during new particle formation events in urban Leipzig, Germany

Rowell, Alex; Brean, James; Beddows, David C.S.; Shi, Zongbo; Kumar, Avinash; Rissanen, Matti; Dal Maso, Miikka; Mettke, Peter; Weinhold, Kay; Merkel, Maik; Harrison, Roy M.

*DOI:*
10.5194/acp-24-10349-2024



*Document Version*
Publisher's PDF, also known as Version of record

*Citation for published version (Harvard):*
Rowell, A, Brean, J, Beddows, DCS, Shi, Z, Kumar, A, Rissanen, M, Dal Maso, M, Mettke, P, Weinhold, K, Merkel, M & Harrison, RM 2024, 'The behaviour of charged particles (ions) during new particle formation events in urban Leipzig, Germany', *Atmospheric Chemistry and Physics*, vol. 24, no. 18, pp. 10349-10361. https://doi.org/10.5194/acp-24-10349-2024

Atmos. Chem. Phys., 24, 10349–10361, 2024
https://doi.org/10.5194/acp-24-10349-2024


Atmospheric Chemistry and Physics
Open Access
EGU



# The behaviour of charged particles (ions) during new particle formation events in urban Leipzig, Germany

**Alex Rowell[1], James Brean[1], David C. S. Beddows[1], Zongbo Shi[1], Avinash Kumar[2], Matti Rissanen[2,3], Miikka Dal Maso[4], Peter Mettke[5], Kay Weinhold[5], Maik Merkel[5], and Roy M. Harrison[1,6]**

[1]School of Geography, Earth and Environmental Sciences, University of Birmingham, Birmingham B15 2TT, United Kingdom
[2]Aerosol Physics Laboratory, Physics Unit, Tampere University, 33720 Tampere, Finland
[3]Department of Chemistry, University of Helsinki, P.O. Box 55, Helsinki, Finland
[4]Department of Physics, Tampere University of Technology, P.O. Box 692, 33100 Tampere, Finland
[5]Leibniz Institute for Tropospheric Research (TROPOS), Atmospheric Chemistry Department (ACD), Permoserstr. 15, 04318 Leipzig, Germany
[6]Department of Environmental Sciences, Faculty of Meteorology, Environment and Arid Land Agriculture, King Abdulaziz University, Jeddah 21589, Saudi Arabia

**Correspondence:** Roy M. Harrison (r.m.harrison@bham.ac.uk)

Received: 12 March 2024 – Discussion started: 3 April 2024
Revised: 16 July 2024 – Accepted: 21 July 2024 – Published: 18 September 2024

**Abstract.** Air ions are electrically charged particles in air. They are ubiquitous in the natural environment and affect the Earth's radiation budget by accelerating the formation and growth of new aerosol particles. Despite this, few datasets exist exploring these effects in the urban environment. A neutral cluster and air ion spectrometer was deployed in Leipzig, Germany, to measure the number size distribution of charged particles from 0.8 to 42 nm, between 27 July and 25 August 2022. Following previous analyses, charged particles were classified into small (0.8–1.6 nm), intermediate (1.6–7.5 nm), and large (7.5–22 nm) fractions by mass diameter, and their mean concentrations (sum of positive and negative polarities) during the campaign were 405, 71.6, and 415 $cm^{-3}$, respectively. The largest peaks in intermediate and large ions were explained by new particle formation (NPF), with intermediate ions correlating well with sulfuric acid dimer. Smaller morning and evening peaks were coincident with black carbon concentrations and attributed to primary emissions. NPF events, observed on 30 % of days, coincided with intense solar radiation and elevated sulfuric acid dimer. Small charged particles were primarily associated with radioactive decay and highest during the early hours, and they are unrelated to primary emissions or NPF. The apparent contributions of charged particles to 3 and 7.5 nm particle formation rates were 5.7 % and 12.7 %, respectively, with mean growth rates of 4.0 nm $h^{-1}$ between 3–7.5 nm and 5.2 nm $h^{-1}$ between 7.5 and 22 nm. The ratio of charged to total particle formation rates at 3 nm suggests a minor role for charged particles in NPF. We conclude that NPF is a primary source of $> 3$ nm ions in our data, with primary emissions being the major source in the absence of NPF.

Published by Copernicus Publications on behalf of the European Geosciences Union.

## 1 Introduction

Atmospheric aerosol particles influence the Earth's energy budget (Carslaw et al., 2013; Quaas et al., 2009), impair visibility (e.g. haze events, aerosol–fog interactions, and cloud formation) (Boutle et al., 2018; Tian et al., 2016), and adversely impact human health through the degradation of air quality (Kelly and Fussell, 2015). The environmental impacts and health effects of aerosol particles are dependent on their number concentration, size, structure, chemical composition, and charge state. These properties, however, vary spatially and temporally (Seinfeld and Pandis, 2016).

New particle formation (NPF) accounts for a large fraction of global aerosol production (Gordon et al., 2017; Spracklen et al., 2010). NPF is a phenomenon observed in many different environments around the world, from pristine remote locations to polluted urban atmospheres (Brean et al., 2021, 2023; Uusitalo et al., 2021; Yao et al., 2018). It is an important atmospheric process wherein gas-phase molecules cluster together and grow to form new aerosol particles. Charged particles can play an important role in the enhancement of these formation and growth processes (Kirkby et al., 2023).

Charged particles, also referred to as air ions, are electrically charged atoms, molecules, clusters of molecules, or aerosols in the atmosphere, which can influence NPF processes. These charged particles can be positively or negatively charged, depending on whether a particle has gained or lost an electron. They can promote the formation of small molecular clusters, enhance their stability, and decrease their evaporation rate (He et al., 2021; Kirkby et al., 2011). Following nucleation and the formation of stable new particles, ion-induced condensation can accelerate particle growth (Svensmark et al., 2017).

Various environmental factors impact the production and removal of air ions and charged particles in the atmosphere. Sources include cosmic rays (Svensmark et al., 2017), radioactive decay (Zhang et al., 2011), traffic (Jayaratne et al., 2014), transmission lines (Jayaratne et al., 2011), volcanic eruptions (Rose et al., 2019), thunderstorms and lightning (Borra et al., 1997), solar radiation (Vana et al., 2008; Wang et al., 2005), vegetation (Wang and Li, 2009), and splashing water (Tammet et al., 2009). Sinks involve redistribution via coagulation with pre-existing aerosol (Mahfouz and Donahue, 2021), losses via ion–ion recombination (Zauner-Wieczorek et al., 2022), and dry deposition (Tammet et al., 2006).

Several studies have investigated the role of ions in the nucleation process, yielding varied results. Manninen et al. (2010) found that contributions of ion-induced nucleation to total particle formation at 2 nm were typically in the range of 1 %–30 % between 12 field sites across Europe. In remote locations, Kulmala et al. (2010) found that contributions were typically significantly less than 10 % in Hyytiälä (Finland), Hohenpeissenberg (Germany), and Melpitz (Germany). In urban locations, contributions were observed at approximately 1.3 % at 1.5 to 2 nm in Helsinki, Finland (Gagné et al., 2012), and 10 % at 3 nm in Brisbane, Australia (Pushpawela et al., 2018). However, few comprehensive analyses of the temporal variation of charged particles, together with their contribution to particle formation and growth in the urban environment, have been published to date.

Here, the daily cycles, sources, and sinks of charged particles, as well as their contributions to new particle formation and growth rates, were investigated in a summertime urban environment. A neutral cluster and air ion spectrometer was deployed at an urban background site in Leipzig, Germany, to measure the mobility distribution of neutral and charged particles, between 27 July and 25 August 2022. The urban background site is located in the Leibniz Institute for Tropospheric Research, a renowned centre specializing in both in situ and remote observations of aerosols and clouds. The air-ion/charged-particle population was classified into small (0.8–1.6 nm mass diameter, 1.1–1.9 nm electrical mobility diameter), intermediate (1.6–7.5 nm mass diameter, 1.9–7.8 nm electrical mobility diameter), and large particles (7.5–22 nm mass diameter, 7.8–22.3 nm electrical mobility diameter) for analysis, following the classification system outlined by Tammet (2006).

## 2 Materials and methods

### 2.1 Site description

Leipzig is located in the German state of Saxony in eastern Germany. Leipzig is the eighth most populated city in Germany, with 0.6 million inhabitants. The measurements were located at the Leibniz Institute for Tropospheric Research (denoted as Leipzig-TROPOS) (51°21′09″ N, 12°26′04″ E; 127 m above mean sea level) within Wissenschaftspark Leipzig (Fig. 1), from 27 July to 25 August 2022. The charged and neutral particle measurements were taken from a laboratory on the fourth floor of an institute building, positioned centrally within the science park, approximately 10 m from ground level. Leipzig-TROPOS is located approximately 100 m from a number of roads with high levels of traffic and is classified as an urban background site. The science park contains other research institutes and related companies; allotted parking bays, including a multi-storey carpark; and greenspace. The park perimeter includes transport infrastructure (including road, rail, and tramways), commercial property (e.g. restaurants, hotels, a petrol station), residential property, on-street parking, and additional greenspace. The solar maximum was at 13:00 LT (local time). Local time was UTC+2, and all times reported here onwards are in local time.

### 2.2 Meteorological conditions

Leipzig has a temperate continental climate. The weather of the city can be highly variable as it is exposed to both cold

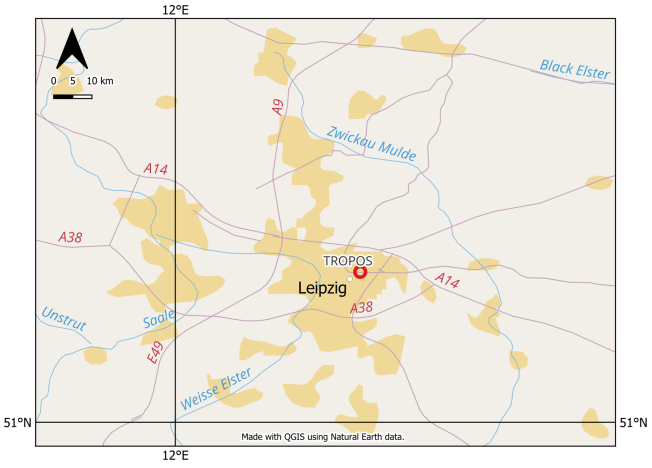


**Figure 1.** Location of the TROPOS site (red marker), approximately 4 km northeast of Leipzig city centre.

and warm air masses, and thunderstorms are not uncommon during the warm season (May through August). Weather-related measurements were taken from a meteorological station on the roof of the same institute building accommodating the air-quality-related instruments at Leipzig-TROPOS. From June to August 2022, persistent heatwaves affected many parts of Europe, including Germany. The mean hourly air temperature during the campaign was 22.4 °C, and the highest hourly air temperature was 37.1 °C recorded on 4 August 2022.

## 2.3 Description of the instruments

### 2.3.1 Neutral cluster and air ion spectrometer

The principle of the neutral cluster and air ion spectrometer (NAIS, Ariel Ltd., Estonia) is described in detail by Mirme and Mirme (2013). An NAIS was used to measure the particle number size distribution (PNSD) of naturally charged particles and also the sum of naturally charged and neutral particles from 0.8–42 nm (3.2–0.0013 $cm^2\,V^{-1}\,s^{-1}$) by their mobilities. From here onwards, we refer to all diameters as mass diameters for consistency with the literature (e.g. Tammet et al., 2006; Ku and de la Mora, 2009). In the case of the charged and neutral particles, the data from 3–42 nm are used, as the charging mechanism for neutral particles causes interference < 3 nm. Neutral and charged measurements will hereon be simply referred to as "total", and the total measurements were taken from the negative column. The instrument was comprised of two multichannel differential mobility analyser (DMA) columns, one for each polarity. Both columns had a software-controlled sample preconditioning unit which allowed the instrument to switch between detecting naturally charged particles or total particles. The sheath air flow rate was approximately 60 $L\,min^{-1}$, and the total sample flow rate was 54 $L\,min^{-1}$ (divided equally between both DMAs). The time resolution per complete distribution was 5 min. Here, we refer to all charged particles measured by the NAIS as "charged particles", which includes charged aerosols, as well as charged molecules and charged clusters of molecules.

### 2.3.2 Custom-built mobility particle size spectrometer

The principle of the mobility particle size spectrometer (MPSS) is described in detail by Wiedensohler et al. (2012). A custom-built MPSS was used to measure the PNSD (from 5 to 800 nm) for the duration of the measurement campaign. The instrument was comprised of a bipolar diffusion charger ($^{85}Kr$ neutralizer), a Vienna-type DMA (electrode length 280 mm), and a condensation particle counter (CPC model 3772, TSI Inc., USA). The sheath air flow rate (5 $L\,min^{-1}$) to sample air flow rate (1 $L\,min^{-1}$) was operated at a ratio of 5 : 1. Both the aerosol sample flow and sheath air flow were actively dried. Particle losses were quantified and accounted for in the final size distribution. The time resolution for a single combined scan, which includes both the increase and subsequent decrease in voltages, was 10 min, and the instrument alternated between measuring the total PNSD and the non-volatile PNSD, giving a measurement of the total PNSD every 20 min.

### 2.3.3 Other instrumentation

The Tampere University nitrate chemical ionization atmospheric pressure interface time-of-flight mass spectrometer (nitrate CI-APi-ToF) was used to measure neutral $H_2SO_4$ and $(H_2SO_4)_nHSO_4^-$ clusters for the duration of the measurement campaign. The instrument is highly sensitive to strongly acidic compounds, as well as compounds with two hydrogen bond donor groups in the gas phase (Hyttinen et al., 2015). The front end consists of a chemical ionization system where a ca. $\sim 8\,L\,min^{-1}$ sample flow is drawn in through a 1 m length 3/4 in. o.d. (outer diameter) stainless-steel tube, where it enters an ionizing chamber. Inside the chamber, a secondary flow is run parallel and concentric to the sample flow, rendering the reaction chamber effectively wall-less. A 10 $cm^3\,min^{-1}$ flow of a carrier gas (in this case $N_2$) is passed over a reservoir of liquid $HNO_3$, entraining vapour which is subsequently ionized to $NO_3^-$ via an X-ray source. The nitrate ions are then guided into the sample flow by an electric field where they charge molecules by clustering or proton transfer. The sample enters the critical orifice at the front end of the instrument at 0.8 $L\,min^{-1}$ and is guided through a series of differentially pumped chambers before it reaches the ToF analyser. Data analysis was carried out in Igor Pro 9. Dried and filtered compressed air was used for the sheath flows.

The instrument was calibrated with respect to sulfuric acid (Kürten et al., 2012). The quantification of sulfuric acid in the

nitrate CI-APi-ToF is as follows:

$$[H_2SO_4] = C \times \ln\left(1 + \left(\frac{H_2SO_4NO_3^- + HSO_4^-}{\sum_{n=0-2}(HNO_3)_nNO_3^-}\right)\right), \quad (1)$$

where $C$ is a calibration constant, here $1.07 \times 10^9\,\mathrm{cm}^{-3}$, for the instrument. Presuming that all collisions between analyte $A$ and the reagent ion result in charging via clustering or deprotonation, the production of charged analytes will continue at the kinetic limit for $H_2SO_4$. Blanks were performed mid-campaign. Blank signals were negligible for all compounds of interest. Black carbon (BC) was measured through the attenuation of 880 nm light with an Aethalometer (AE33, Magee Scientific, USA) using the default mass absorption coefficient.

### 2.4 Condensation sink, formation, and growth rates

NPF events were identified visually based on the time evolution of the PNSD plotted as contour plots using the criteria of Dal Maso et al. (2005). Measurement days were classified into three categories: NPF, undefined, and non-NPF event according to methods described by Dal Maso et al. (2005). NPF event days were classified as such when days showed both particle formation and growth. Equally, undefined days were assigned when days satisfied some but not all of the aforementioned criteria (i.e. a new but non-persistent mode or no clear signs of growth). Lastly, non-NPF event days were grouped as such when the total PNSD data showed no clear indication of new particle formation.

Each plot contained data spanning 24 h and ranging from 0.8–42 nm (charged PNSD from the NAIS) and 3–800 nm (neutral and charged PNSD from the NAIS and custom-built MPSS, utilizing the NAIS $< 20$ nm and the MPSS $> 20$ nm). An example plot is given in Fig. S1 in the Supplement. All NPF signatures were seen simultaneously in the PNSD and charged PNSD simultaneously. Each day was plotted using a perceptually uniform, high-contrast colour palette (Mikhailov, 2019).

The condensation sink (CS) represents the rate at which a vapour-phase molecule will collide with pre-existing particle surface, and this parameter was calculated from the MPSS data as follows (Kulmala et al., 2012):

$$\mathrm{CS} = 2\pi D \cdot \sum_{d_\mathrm{p}} \beta_{m,d_\mathrm{p}} \cdot d_\mathrm{p} \cdot N_{d_\mathrm{p}}, \quad (2)$$

where $D$ is the diffusion coefficient of the diffusing vapour (assumed to be sulfuric acid), $\beta_m$ is a transition regime correction, $d_\mathrm{p}$ is particle diameter, and $N_{d_\mathrm{p}}$ is the number of particles at diameter $d_\mathrm{p}$. The formation rate of new particles at size $d_\mathrm{p}$ ($J_{d_\mathrm{p}}$) is calculated as follows, presuming a homogeneous air mass:

$$J_{d_\mathrm{p}} = \frac{\mathrm{d}N_{d_\mathrm{p}}}{\mathrm{d}t} + \mathrm{CoagS}_{d_\mathrm{p}} \cdot N_{d_\mathrm{p}} + \frac{\mathrm{GR}}{\Delta d_\mathrm{p}} \cdot N_{d_\mathrm{p}}, \quad (3)$$

where the first term on the right-hand side represents the rate at which particles enter the size $d_\mathrm{p}$, and the second term refers to losses from this size by coagulation ($\mathrm{CoagS}_{d_\mathrm{p}}$ being the coagulation sink at size $d_\mathrm{p}$, and $N_{d_\mathrm{p}}$ being the number of particles at size $d_\mathrm{p}$, calculated according to Cai and Jiang, 2017), with the third term referring to losses from this size by growth. When calculating the formation rate, instead of using a single particle size, a range is used. In this paper we use two ranges: 3–7.5 nm for 3 nm particles and 7.5–22 nm for 7.5 nm particles. These sizes were chosen for consistency with the size cuts used for the rest of the analyses. The formation rate of charged particles involves two additional terms and is as follows:

$$J^{\mp}_{d_\mathrm{p}} = \frac{\mathrm{d}N^{\mp}_{d_\mathrm{p}}}{\mathrm{d}t} + \mathrm{CoagS}_{d_\mathrm{p}} \cdot N^{\mp}_{d_\mathrm{p}} + \frac{\mathrm{GR}}{\Delta d_\mathrm{p}} \cdot N^{\mp}_{d_\mathrm{p}} + \alpha \cdot N^{\mp}_{d_\mathrm{p}} \cdot N^{\pm}_{< d_{\text{p-upper}}} - \beta \cdot N_{d_\mathrm{p}} \cdot N^{\mp}_{< d_{\text{p-lower}}}, \quad (4)$$

where the fourth term accounts for the loss of charged particles due to their recombination with other charged particles of the opposite polarity below the upper bound of $d_\mathrm{p}$, and the fifth term accounts for the gain of charged particles caused by the attachment of charged particles below the lower bound of $d_\mathrm{p}$ with neutral clusters (Yan et al., 2018). The growth rate (GR) of new particles, which is the change of $d_\mathrm{p}$ over time of new particles, is calculated here by the mode-fitting method (Kulmala et al., 2012).

## 3 Results and discussion

### 3.1 Number concentrations of charged particles

Table 1 shows a statistical summary of small-, intermediate-, and large-charged-particle concentrations at Leipzig-TROPOS. Mean number concentrations of small charged particles (0.8–1.6 nm) were 305 and 100 $\mathrm{cm}^{-3}$ for positive and negative polarities, respectively. Observed concentrations are comparable with, albeit on the lower end of, the typical tropospheric range reported by Hirsikko et al. (2011). The comparatively low concentrations are in line with the higher coagulation sink for small particles in the urban environment, which is expected to reduce the average concentration. The positive particle concentrations are roughly a factor of 3 greater than the negative particle concentrations, and this is consistent across the 5 %–95 % spread, so results are not attributable to spikes in positive charged particles (see mean charged PNSD in Fig. 2a). Similar disparities between small charged particles of opposing polarities have been documented in the literature. A measurement campaign in Saare County, Estonia, between July and September 1984 reported mean concentrations of positively and negatively charged small particles of 261 and 173 $\mathrm{cm}^{-3}$, respectively (Hõrrak, 1987). The imbalance is believed to be caused by the Earth's negatively charged surface impacting the distribution of charged particles, referred to as the electrode effect

**Table 1.** Statistical summary of small (0.8–1.6 nm), intermediate (1.6–7.5 nm), and large (7.5–22 nm) charged-particle number concentrations per $cm^{-3}$. Data coverage: 27 July 2022 14:00 to 25 August 2022 08:00 (UTC) using hourly means.

| | Mean | Median | 5 %–95 % |
|---|---|---|---|
| Small (+) | 305 | 299 | 193–451 |
| Small (−) | 100 | 96.2 | 45.3–173 |
| Intermediate (+) | 30.7 | 12.4 | 1.36–132 |
| Intermediate (−) | 40.9 | 18.9 | 6.24–174 |
| Large (+) | 205 | 147 | 43.8–611 |
| Large (−) | 210 | 152 | 54.9–620 |

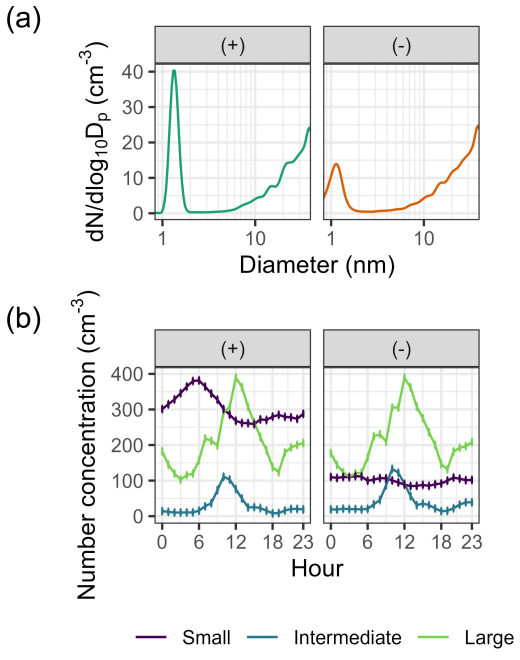


**Figure 2.** **(a)** Mean size distribution of positively and negatively charged particles between 0.8 and 22 nm. **(b)** Mean diurnal cycles of small (0.8–1.6 nm), intermediate (1.6–7.5 nm), and large (7.5–22 nm) charged particles. The vertical lines represent the standard error of the mean.

(Hoppel, 1967; Hõrrak et al., 2003). This effect is closest to the ground and tapers off strongly at a height of metres (Hõrrak et al., 2003). This may also be due to a charged surface on the wall near the inlet or the inlet itself.

Mean concentrations of intermediate charged particles (1.6–7.5 nm), on the other hand, were comparatively very low. Mean number concentrations of intermediate charged particles were 30.7 and 40.9 $cm^{-3}$ for positive and negative polarities, respectively. Negative particles show greater spread, with the lower 5 % and lower mean counts possibly also attributable to the electrode effect. Observations are very similar to annual mean concentrations (35–40 $cm^{-3}$ for each polarity) recorded between April 2010 and November 2011 in Tartu, Estonia, by Tammet et al. (2014). Although, they are approximately 2 times higher (depending on polarity, with higher negative concentrations) than mean concentrations recorded between June 2009 and October 2010 in Paris, France, by Dos Santos et al. (2015). The differences between these studies may be explained by the proximity to and density of the surrounding transport infrastructure (see Sect. 3.2), photochemical processes (see Sect. 3.5), and length of campaign period.

Much like intermediate charged particles, there was little difference in mean concentrations between the opposing polarities of large charged particles (7.5–22 nm). However, mean concentrations of large charged particles (during the whole campaign) were considerably higher than intermediate charged particles. Mean number concentrations were 210 and 205 $cm^{-3}$ for positive and negative polarities, respectively, and were approximately 5–6 times higher (depending on polarity, higher for positive particles) than intermediate charged particles. The spread in large ion counts is similar between positive and negative charged particles, and the relative magnitude of this spread is similar to the intermediate ions.

### 3.2 Diurnal cycles of charged particles

Figure 2b shows the mean diurnal cycles of small, intermediate, and large charged particles at Leipzig-TROPOS. Small-charged-particle concentrations peaked in the early morning (05:00–06:00), decreased into the afternoon (11:00–13:00), and increased into the night. Such observations are comparable to other studies in Pune, India (Dhanorkar and Kamra, 1994); Tumbarumba, Australia (Suni et al., 2008); and Paris, France (Dos Santos et al., 2015), and they may be attributed to fluctuations in boundary layer mixing height and the accumulation of radioactive gases (e.g. radon). Concentrations of small charged particles increased prior to the below-mentioned peaks in intermediate- and large-charged-particle concentrations and decreased thereafter. Diurnal cycles suggest that small charged particles arise primarily from natural processes and are quickly lost via recombination and attachment to larger aerosols. The main natural ion production processes are cosmic radiation and radioactive decay. Cosmic ray intensity is fairly constant throughout the lower atmosphere (Mercer and Wilson, 1965), while the variations in radon concentrations are attributable to boundary layer dynamics (Čeliković et al., 2023). The diurnal variation we observe is therefore likely to be a combination of boundary layer height changes affecting the radon concentrations (and therefore source strength) and variations in particle number surface area altering loss rates due to coagulation due to both boundary layer height changes and primary and secondary particle emissions.

Intermediate-charged-particle concentrations peaked several hours after the initial peak in small charged particles (10:00) and again later in the day (22:00). Similarly, large-charged-particle concentrations peaked at midday (12:00),

and lower peaks were observed in the morning (07:00–08:00) and in the evening/night-time (23:00). Before-midday and midday peaks (10:00 for intermediate, 12:00 for large) in both classifications coincided with intense solar radiation (see Sect. 3.4) and occurred when NPF events were observed (see Sect. 3.5). Lower peaks coincided with busy road traffic periods and economic activities, known to emit high quantities of positive and negative charged particles (Jayaratne et al., 2010, 2014; Thomas et al., 2024). Pollution-related peaks appeared more pronounced in the large-charged-particle fraction. Diurnal cycles suggest that photochemistry and local air pollution dominate intermediate- and large-charged-particle production, with the latter contributing more significantly to large-charged-particle concentrations.

### 3.3 Frequency of new particle formation

A total of 9 NPF, 6 undefined, and 15 non-NPF event days were identified across the 30 d measurement campaign at Leipzig-TROPOS. The frequency of NPF event days (30 %) was comparable with frequencies from long-term analysis of summertime data at this site (Bousiotis et al., 2021).

### 3.4 Meteorology and charged particles

Figure 3 shows the correlation coefficients between charged particles in different diameter classifications and meteorological variables at Leipzig-TROPOS. Individual scatterplots are available in Fig. S2. Solar radiation and air temperature exhibited negative correlations with small charged particles but positive correlations with intermediate and large charged particles. Conversely, relative humidity showed positive correlations with small charged particles and negative correlations with intermediate and large charged particles. Air temperature is typically elevated when solar radiation is high, and relative humidity is typically inversely related with air temperature (Seinfeld and Pandis, 2016). Fluctuations in boundary layer mixing height, the accumulation of radioactive gases, and the CS (discussed in Sect. 3.2) are believed to have influenced the small-charged-particle fraction. Mixing layer height is influenced by air temperature, with cooler morning temperatures theoretically limiting vertical mixing (Seinfeld and Pandis, 2016) and inadvertently enhancing small-charged-particle concentrations.

### 3.5 Diurnal cycles of charged particles during new particle formation

Figure 4a, c, and e show the mean diurnal cycles of small, intermediate, and large charged particles on NPF, undefined, and non-NPF event days at Leipzig-TROPOS. On NPF event days, diurnal maxima of small charged particles were observed between 05:00 and 08:00 and minima between 14:00 and 16:00. These diurnal cycles are unrelated to NPF. Diurnal maxima of intermediate and large charged particles were observed at 10:00 and 12:00, respectively. Time gaps between maximum concentrations of intermediate and large charged particles (approximately 2 h) likely indicate growth between size classifications, a phenomenon not observed on non-NPF event days (alternative graphic presented in Fig. S4). Comparable time gaps have been observed in both urban (Dos Santos et al., 2015) and rural (Hõrrak et al., 2003) settings. Small-charged-particle concentrations were lower on NPF event days compared to non-NPF event days, consistent with findings in rural areas (Gagné et al., 2010; Hõrrak et al., 2003), possibly due to stronger vertical mixing and a deeper boundary layer. In contrast, maximum concentrations of intermediate and large charged particles were approximately 4.0–4.4 and 3.6–3.7 times higher (depending on polarity, higher for negative particles), respectively, on NPF event days compared to non-NPF event days.

The mean diurnal cycles of black carbon, sulfuric acid ($H_2SO_4$) dimer, and condensation sink (CS) concentrations on NPF, undefined, and non-NPF event days at Leipzig-TROPOS are shown in Fig. 4b, d, and f. BC concentrations were generally lower in the morning and into the early evening, and they were noticeably higher in the late evening/night-time on NPF event days compared to non-NPF event days. Morning and late evening/night-time peaks occurred synchronously with peaks in large charged particles. BC is often used as a proxy for traffic-related air pollution and other combustion-related activities (Seinfeld and Pandis, 2016). Peaks in BC were synchronous with peaks in the CS due to the high surface area of BC-containing particles. Maximum $H_2SO_4$ dimer concentrations peaked synchronously with intermediate-charged-particle concentrations. In the nitrate CI-APi-ToF, the $H_2SO_4$ dimer is a representation of atmospheric $H_2SO_4$. $HSO_4^-$, larger atmospheric sulfuric acid–base clusters which undergo evaporation due to chemical ionization, and some ion–molecule pairing in the front of the chemical ionization mass spectrometer (CIMS) inlet (Almeida et al., 2013) and is considered a good proxy for the occurrence of NPF in urban environments (Yao et al., 2018). $H_2SO_4$ dimer is highest on NPF days, while BC is low. BC peaks in the evening time, possibly due to a shallow nocturnal boundary layer on these days. CS on event days is similar to non-event days, indicating that the key difference is $H_2SO_4$ dimer source strength. A CS peak approximately 5 h after the $H_2SO_4$ dimer peak on NPF event days reflects the growing mode of new particles contributing appreciably to surface area.

Concentrations of other acids ($HIO_3$, methanesulfonic acid) are an order of magnitude lower than $H_2SO_4$ concentrations, and so $H_2SO_4$ is the most likely candidate for the driver of NPF in this area. Temperatures were high ($\sim 30\,^{\circ}C$) during the campaign, and it is unlikely that oxygenated organic molecules can drive particle formation in these data (Simon et al., 2020). The correlation between $H_2SO_4$ dimer and charged-particle concentration (Fig. 5) shows that there is no statistically significant correlation between $H_2SO_4$ dimer and

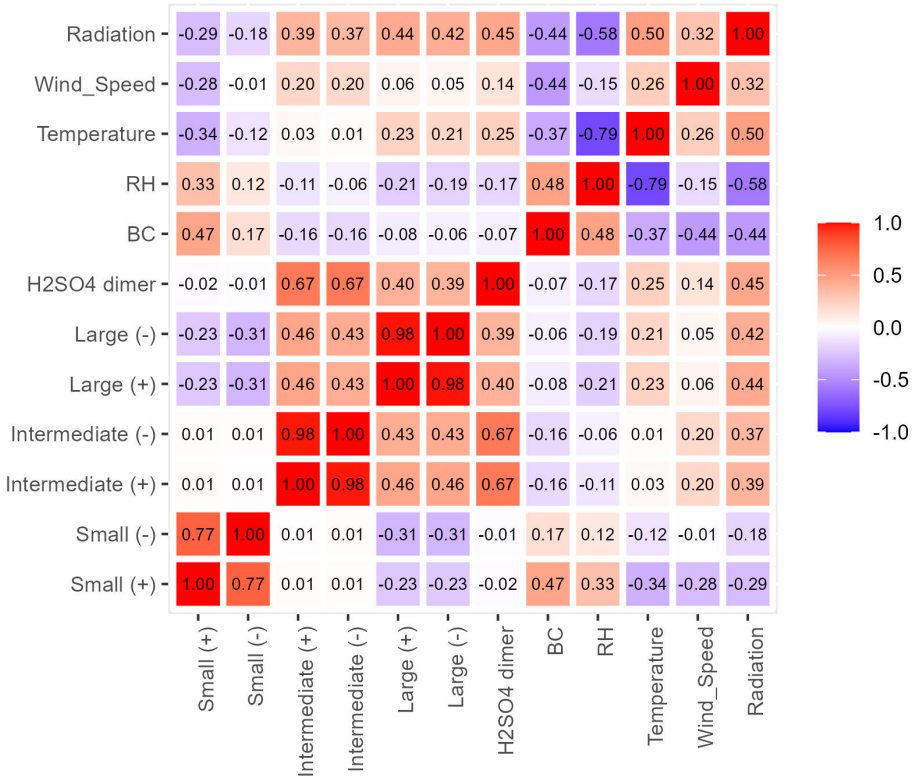


**Figure 3.** Pearson correlation matrix heatmap of meteorological variables (solar radiation, air temperature, relative humidity, and wind speed) and small, intermediate, large, and total charged particles (of both polarities). Also included are $H_2SO_4$ dimer and BC. Warm colours (red) represent positive correlations, whereas cold colours (blue) represent negative correlations. Correlation strength ranges from $-1$ to $+1$. The shade indicates the strength of the correlation, with darker shades indicating stronger correlations. Data coverage: 27 July 2022 14:00 to 25 August 2022 08:00 (UTC) using hourly means. Individual scatterplots are available in Fig. S2.

small charged particles, while the correlation with intermediate and large ions is statistically significant. The correlation is strongest for the intermediate ions, which peak coincidentally with $H_2SO_4$ dimer, which is coincident with high solar radiation (Figs. 3, S3). Particle formation is accelerated by ionizing radiation (Kirkby et al., 2011, 2023), and a fraction of these new particles will be charged or will pick up charge as they grow. NPF occurred on days with higher temperatures and solar radiation (Fig. S3), which is typical of ground-level NPF (Kerminen et al., 2018; Lee et al., 2019). High temperatures can increase cluster evaporation rates, but this can be offset by the presence of ions (Lee et al., 2019), although this is dependent on cluster composition (Kirkby et al., 2023). We attribute these midday peaks in intermediate and large ions to NPF, which is likely driven by sulfuric acid, and argue that NPF is the major source of charged particles in this campaign (Figs. 2b, S3). Primary emissions of intermediate and charged ions will be coincident with BC emissions (Thomas et al., 2024).

Undefined and non-NPF days occur when $H_2SO_4$ dimer is low. Undefined events are seen when CS is high, and BC is higher than NPF event days, likely due to traffic emissions, and non-event days occur when BC and CS are lower. Non-NPF days are possibly observed on these days due to low concentrations of precursors. The morning and evening peaks in intermediate and large ions are coincident with peaks in BC concentrations and are therefore explicable by primary traffic emissions (Thomas et al., 2024), and we argue that primary emissions are the second largest source of intermediate and large ions in our data.

### 3.6 Charged particles and particle formation rates

Figure 6a and b show the apparent formation rates ($J$) of 3 and 7.5 nm charged particles (sum of both negative and positive particle formation rates; $J_{3-7.5}^{\text{charged}}$ and $J_{7.5-22}^{\text{charged}}$) and total particles ($J_{3-7.5}^{\text{total}}$ and $J_{7.5-22}^{\text{total}}$) during NPF event days at Leipzig-TROPOS. Figure 6c shows the diurnal cycle of these rates. The ratio of $J^{\text{positive}} : J^{\text{negative}}$ is 0.9. Notably, the apparent $J$ values of charged particles increased with aerosol size. The mean $J$ values for 3 and 7.5 nm charged particles during NPF were 0.165 and 0.326 $\text{cm}^{-3}\,\text{s}^{-1}$, respectively, with mean values of $J_{7.5-22}^{\text{charged}}$ approximately 2 times higher than $J_{3-7.5}^{\text{charged}}$. These compare with mean $J$ values of 3 and 7.5 nm total particles during NPF of 7.21 and

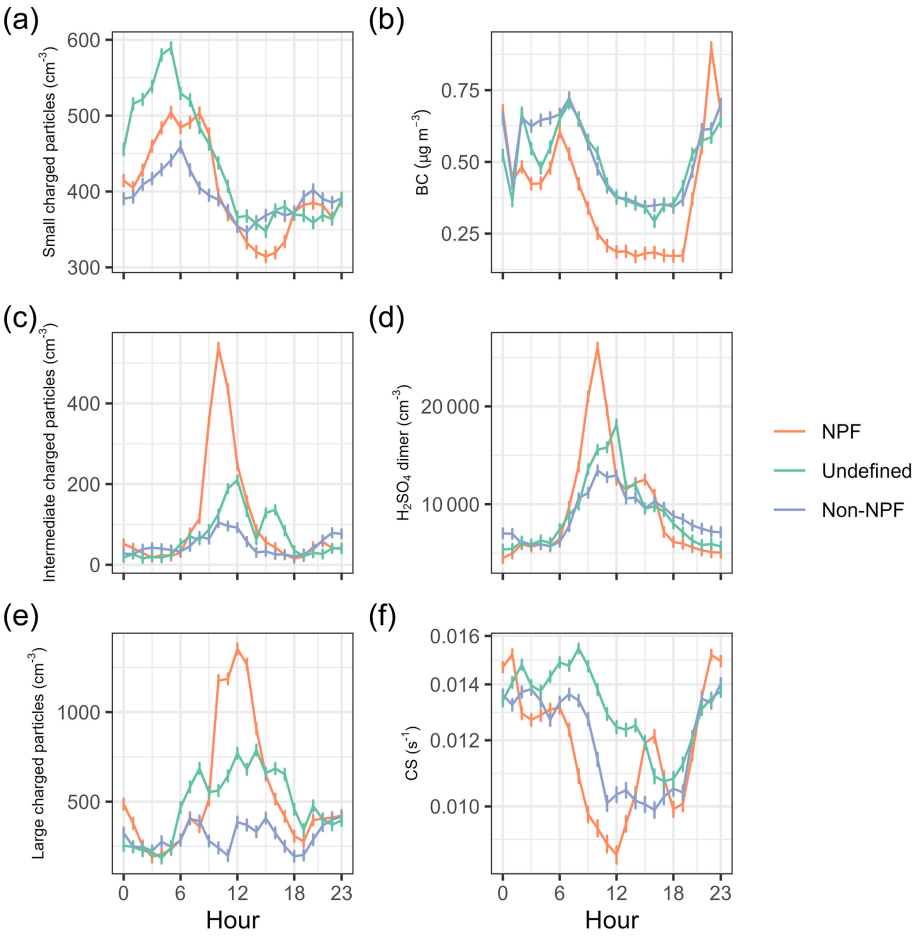


**Figure 4.** Mean diurnal cycles of **(a)** small (0.8–1.6 nm), **(c)** intermediate (1.6–7.5 nm), and **(e)** large (7.5–22 nm) charged particles, as well as **(b)** BC, **(d)** $H_2SO_4$ dimer, and **(f)** CS on new particle formation (NPF), undefined, and non-NPF event days. The vertical lines represent the standard error of the mean.

1.47 cm$^{-3}$ s$^{-1}$, respectively, with mean values of $J^{\text{total}}_{7.5-22}$ approximately 0.68 times those of $J^{\text{total}}_{3-7.5}$. The aforementioned $J$ values are within the observed tropospheric ranges for charged and total particles reported by Hirsikko et al. (2011). When considering the calculated ratios of $J^{\text{charged}} / J^{\text{total}}$ in the respective size ranges, the apparent mean contributions of charged particles to 3 and 7.5 nm total particle formation were 5.7 % and 12.7 %, respectively. $J^{\text{total}}_{3-7.5}$ is higher than $J^{\text{total}}_{7.5-22}$, which is typical, as new particles are lost as they grow from 3 to 7.5 nm. However, $J^{\text{charged}}_{3-7.5}$ is lower than $J^{\text{charged}}_{7.5-22}$. We attribute this to charging of growing aerosol by the condensation of smaller charged particles, and this is consistent with the low concentrations of intermediate charged particles (Fig. 2a, Table 1). The diurnal cycle in $J$ shows a peak that is coincident with the peaks in $H_2SO_4$ dimer (Fig. 4) and intermediate charged ion concentrations (Fig. 4).

Large charged particles are more likely to act as a sink because of their greater surface area. In comparison, smaller charged particles are more susceptible to ion–ion recombination due to higher mobility. This recombination process, wherein two oppositely charged particles combine and neutralize each other, accounted for in Eq. (4), can impact the abundance of smaller charged particles, influencing their ability to contribute to nucleation and particle formation in the atmosphere. It would be reasonable to view $J^{\text{charged}}_{3-7.5}$ as an upper limit to ion-induced nucleation, while larger charged particles appear to have a substantial contribution from charges acquired subsequently. The apparent contributions are comparable with ranges from other European field sites (1 %–30%), covering a wide variety of environments reported by Manninen et al. (2010). Nevertheless, observed ratios of charged to total particles in the size range impacted by NPF suggest charged particles play a minor role compared to neutral particles in NPF at Leipzig-TROPOS in our data.

### 3.7 Charged-particle growth rates

Figure 6d shows growth rates (GRs) of charged particles within diameters 3–7.5 and 7.5–22 nm during NPF event

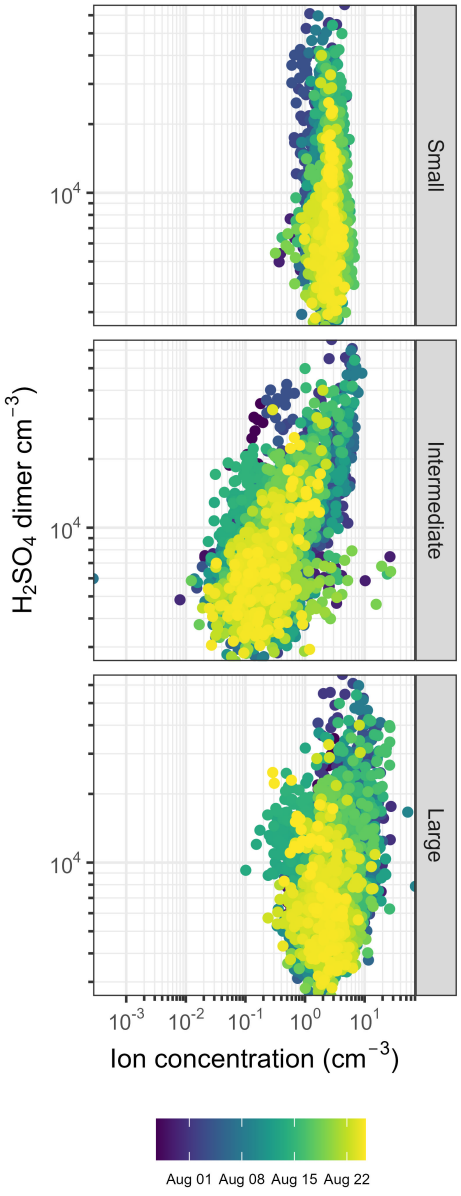


**Figure 5.** Correlation of $H_2SO_4$ dimer with small, intermediate, and large ions, coloured by date. The $R^2$ values are 0.0014, 0.27, and 0.079, respectively; the $p$ values are $> 0.05$, $< 0.05$, and $< 0.05$, respectively.

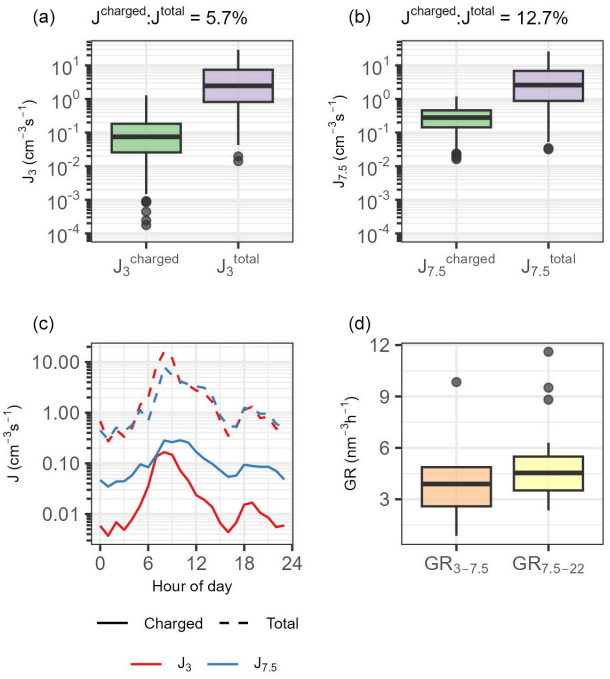


**Figure 6.** Apparent formation rates of **(a)** 3–7.5 nm charged particles (left) and total particles (right) and **(b)** 7.5–22 nm charged particles (left) and total particles (right). Calculated from nine new particle formation (NPF) event days using 10 min means. **(c)** The diurnal cycle in formation rates on NPF days and **(d)** growth rates (GR) of 3–7.5 and 7.5–22 nm charged particles. The coloured rectangle represents the middle 50 % of the data, with the central horizontal line indicating the median value. The whiskers (vertical lines) extending from the rectangle show the spread of the data. Data points beyond the whiskers show outliers.

days at Leipzig-TROPOS. Consistent with previous studies (Manninen et al., 2010; Dos Santos et al., 2015; Svensmark et al., 2017), the GR of charged particles generally increased with size. This observation is attributed to the Kelvin effect, where the condensational growth of smaller particles is driven by a limited number of very low volatility compounds. In contrast, the growth of larger particles is influenced by a greater number of molecules, including oxygenated organic molecules (Kirkby et al., 2023). Contrary to the $J$ values discussed in Sect. 3.6, GRs of charged particles are expected to align more closely with that of neutral particles (Svensmark et al., 2017). Small discrepancies may arise due to the enhanced condensation of ionized gases and improved coagulation resulting from charge–charge effects (Svensmark et al., 2017). Mean GRs of 3–7.5 and 7.5–22 nm charged particles were 4.0 and 5.2 nm h$^{-1}$, respectively. In comparison, Manninen et al. (2010) reported median GRs from various European field sites as 4.3 and 5.4 nm h$^{-1}$ for 3–7 and 7–20 nm charged particles, respectively.

## 4 Conclusion

The charged and total PNSDs were measured from 27 July to 25 August 2022 using an NAIS in urban Leipzig to understand the sources, sinks, and dynamics of charged particles. Throughout the measurement campaign, small (0.8–1.6 nm), intermediate (1.6–7.5 nm), and large (7.5–22 nm) charged particles were ever-present. Small-charged-particle concentrations were consistent with observations in the existing literature. A clear disparity was evident between positive and negative polarities, attributed to the Earth's electrode effect. Despite these differences, their diurnal cycles were very similar. Small-charged-particle concentrations peaked in the

early morning, decreased into the afternoon, and rose again into the night. These fluctuations are believed to be related to changes in the boundary layer mixing height and the accumulation of radioactive gases. Maximum concentrations of intermediate and large charged particles were observed in the morning hours, with the latter peaking closer to midday. Local air pollution had a more substantial impact on larger charged particles compared to small and intermediate charged particles, indicated by synchronous peaks in black carbon concentrations, and we argue that primary emissions are a major contributor to intermediate and large ions.

NPF events were identified on 30 % of measurement days, occurring under intense solar radiation, significant diurnal temperature fluctuations, and decreasing relative humidity from morning to afternoon. Notably, small-charged-particle concentrations were typically lower on NPF event days compared to non-NPF event days. Peak concentrations of intermediate and large charged particles were approximately 4.0–4.4 and 3.6–3.7 times higher (depending on polarity, higher for negative particles), respectively, on NPF event days compared to non-NPF event days. $H_2SO_4$ dimer concentrations were elevated on NPF event days and peaked synchronously with intermediate-charged-particle concentrations.

The apparent contributions of charged particles to 3 and 7.5 nm particle formation were 5.7 % and 12.7 %, respectively, with mean growth rates of 4.0 and 5.2 nm $h^{-1}$. Both the apparent formation and growth rates of charged particles increased with aerosol size and were found to be comparable with ranges reported in previous studies. The ratio of total to charged nanoparticles and small magnitude of $J_{3-7.5}^{\text{charged}}$ suggest that ion-induced processes play a minor role compared to neutral particles in NPF at Leipzig-TROPOS in this campaign.

**Code availability.** The code will be made available on reasonable request.

**Data availability.** Data supporting this publication are openly available from the UBIRA eData repository at https://doi.org/10.25500/edata.bham.00001073 (Harrison et al., 2024).

**Supplement.** The supplement related to this article is available online at: https://doi.org/10.5194/acp-24-10349-2024-supplement.

**Author contributions.** Conceptualization – AR, JB; data curation – AR, JB; formal analysis – AR, JB; funding acquisition – RMH, ZS; investigation – AR, JB; methodology – AR, JB; project administration – RMH; resources – MR, MDM, PM, KW, MM; software – AR, JB; supervision – RMH, ZS; visualization – AR, JB; writing (original draft preparation) – AR; writing (review and editing) – AR, JB, DCSB, ZS, AK, MR, MDM, PM, KW, RMH.

**Competing interests.** The contact author has declared that none of the authors has any competing interests.

**Disclaimer.** Publisher's note: Copernicus Publications remains neutral with regard to jurisdictional claims made in the text, published maps, institutional affiliations, or any other geographical representation in this paper. While Copernicus Publications makes every effort to include appropriate place names, the final responsibility lies with the authors.

**Acknowledgements.** The University of Birmingham would like to express sincere appreciation to the TROPOS team for their gracious hosting and invaluable assistance during our measurement campaign. Support from the doctoral school of the Faculty of Engineering and Natural Sciences of Tampere University is gratefully acknowledged.

**Financial support.** This project was funded by the UK Natural Environment Research Council (grant no. NE/V001523/1 NPF-Urban). This project has received funding from the European Research Council under the European Union's Horizon 2020 research and innovation programme under grant no. 101002728 (ERC Consolidator Grant Project ADAPT). Support was received from the Research Council of Finland (grant nos. 353836 and 346373) as well as its flagship programme (decision nos. 337551 and 357903).

**Review statement.** This paper was edited by Yafang Cheng and reviewed by three anonymous referees.

## References

Almeida, J., Schobesberger, S., Kürten, A., Ortega, I. K., Kupiainen-Määttä, O., Praplan, A. P., Adamov, A., Amorim, A., Bianchi, F., Breitenlechner, M., David, A., Dommen, J., Donahue, N. M., Downard, A., Dunne, E., Duplissy, J., Ehrhart, S., Flagan, R. C., Franchin, A., Guida, R., Hakala, J., Hansel, A., Heinritzi, M., Henschel, H., Jokinen, T., Junninen, H., Kajos, M., Kangasluoma, J., Keskinen, H., Kupc, A., Kurtén, T., Kvashin, A. N., Laaksonen, A., Lehtipalo, K., Leiminger, M., Leppä, J., Loukonen, V., Makhmutov, V., Mathot, S., McGrath, M. J., Nieminen, T., Olenius, T., Onnela, A., Petäjä, T., Riccobono, F., Riipinen, I., Rissanen, M., Rondo, L., Ruuskanen, T., Santos, F. D., Sarnela, N., Schallhart, S., Schnitzhofer, R., Seinfeld, J. H., Simon, M., Sipilä, M., Stozhkov, Y., Stratmann, F., Tomé, A., Tröstl, J., Tsagkogeorgas, G., Vaattovaara, P., Viisanen, Y., Virtanen, A., Vrtala, A., Wagner, P. E., Weingartner, E., Wex, H., Williamson, C., Wimmer, D., Ye, P., Yli-Juuti, T., Carslaw, K. S., Kulmala, M., Curtius, J., Baltensperger, U., Worsnop, D. R., Vehkamäki, H., and Kirkby, J.: Molecular understanding of sulphuric acid–amine particle nucleation in the atmosphere, Nature, 502, 359–363, https://doi.org/10.1038/nature12663, 2013.

Borra, J.-P., Roos, R. A., Renard, D., Lazar, H., Goldman, A., and Goldman, M.: Electrical and chemical consequences of point discharges in a forest during a mist and a thunderstorm,

J. Phys. D. Appl. Phys., 30, 84, https://doi.org/10.1088/0022-3727/30/1/011, 1997.

Bousiotis, D., Pope, F. D., Beddows, D. C. S., Dall'Osto, M., Massling, A., Nøjgaard, J. K., Nordstrøm, C., Niemi, J. V., Portin, H., Petäjä, T., Perez, N., Alastuey, A., Querol, X., Kouvarakis, G., Mihalopoulos, N., Vratolis, S., Eleftheriadis, K., Wiedensohler, A., Weinhold, K., Merkel, M., Tuch, T., and Harrison, R. M.: A phenomenology of new particle formation (NPF) at 13 European sites, Atmos. Chem. Phys., 21, 11905–11925, https://doi.org/10.5194/acp-21-11905-2021, 2021.

Boutle, I., Price, J., Kudzotsa, I., Kokkola, H., and Romakkaniemi, S.: Aerosol–fog interaction and the transition to well-mixed radiation fog, Atmos. Chem. Phys., 18, 7827–7840, https://doi.org/10.5194/acp-18-7827-2018, 2018.

Brean, J., Dall'Osto, M., Simó, R., Shi, Z., Beddows, D. C. S., and Harrison, R. M.: Open ocean and coastal new particle formation from sulfuric acid and amines around the Antarctic Peninsula, Nat. Geosci., 14, 383–388, https://doi.org/10.1038/s41561-021-00751-y, 2021.

Brean, J., Beddows, D. C. S., Harrison, R. M., Song, C., Tunved, P., Ström, J., Krejci, R., Freud, E., Massling, A., Skov, H., Asmi, E., Lupi, A., and Dall'Osto, M.: Collective geographical ecoregions and precursor sources driving Arctic new particle formation, Atmos. Chem. Phys., 23, 2183–2198, https://doi.org/10.5194/acp-23-2183-2023, 2023.

Cai, R. and Jiang, J.: A new balance formula to estimate new particle formation rate: reevaluating the effect of coagulation scavenging, Atmos. Chem. Phys., 17, 12659–12675, https://doi.org/10.5194/acp-17-12659-2017, 2017.

Carslaw, K. S., Lee, L. A., Reddington, C. L., Pringle, K. J., Rap, A., Forster, P. M., Mann, G. W., Spracklen, D. V, Woodhouse, M. T., Regayre, L. A., and Pierce, J. R.: Large contribution of natural aerosols to uncertainty in indirect forcing, Nature, 503, 67–71, https://doi.org/10.1038/nature12674, 2013.

Čeliković, I., Pantelić, G., Vukanac, I., Krneta Nikolić, J., Živanović, M., Cinelli, G., Gruber, V., Baumann, S., Quindos Poncela, L. S., and Rabago, D.: Outdoor Radon as a Tool to Estimate Radon Priority Areas–A Literature Overview, Int. J. Env. Res. Pub. He., 19, 662, https://doi.org/10.3390/ijerph19020662, 2022.

Dal Maso, M., Kulmala, M., Riipinen, I., Wagner, R., Hussein, T., Aalto P., P., and Lehtinen K., E. J.: Formation and growth of fresh atmospheric aerosols: eight years of aerosol size distribution data from SMEAR II, Hyytiala, Finland, Boreal Environ. Res., 10, 323–336, 2005.

Dhanorkar, S. and Kamra, A. K.: Diurnal variation of ionization rate close to ground, J. Geophys. Res.-Atmos., 99, 18523–18526, https://doi.org/10.1029/94JD01335, 1994.

Dos Santos, V. N., Herrmann, E., Manninen, H. E., Hussein, T., Hakala, J., Nieminen, T., Aalto, P. P., Merkel, M., Wiedensohler, A., Kulmala, M., Petäjä, T., and Hämeri, K.: Variability of air ion concentrations in urban Paris, Atmos. Chem. Phys., 15, 13717–13737, https://doi.org/10.5194/acp-15-13717-2015, 2015.

Gagné, S., Nieminen, T., Kurtén, T., Manninen, H. E., Petäjä, T., Laakso, L., Kerminen, V.-M., Boy, M., and Kulmala, M.: Factors influencing the contribution of ion-induced nucleation in a boreal forest, Finland, Atmos. Chem. Phys., 10, 3743–3757, https://doi.org/10.5194/acp-10-3743-2010, 2010.

Gagné, S., Leppä, J., Petäjä, T., McGrath, M. J., Vana, M., Kerminen, V.-M., Laakso, L., and Kulmala, M.: Aerosol charging state at an urban site: new analytical approach and implications for ion-induced nucleation, Atmos. Chem. Phys., 12, 4647–4666, https://doi.org/10.5194/acp-12-4647-2012, 2012.

Gordon, H., Kirkby, J., Baltensperger, U., Bianchi, F., Breitenlechner, M., Curtius, J., Dias, A., Dommen, J., Donahue, N. M., Dunne, E. M., Duplissy, J., Ehrhart, S., Flagan, R. C., Frege, C., Fuchs, C., Hansel, A., Hoyle, C. R., Kulmala, M., Kürten, A., Lehtipalo, K., Makhmutov, V., Molteni, U., Rissanen, M. P., Stozkhov, Y., Tröstl, J., Tsagkogeorgas, G., Wagner, R., Williamson, C., Wimmer, D., Winkler, P. M., Yan, C., and Carslaw, K. S.: Causes and importance of new particle formation in the present-day and preindustrial atmospheres, J. Geophys. Res.-Atmos., 122, 8739–8760, https://doi.org/10.1002/2017JD026844, 2017.

Harrison, R. M., Rowell, A., and Brean, J.: Research data supporting "The behaviour of charged particles (ions) during new particle formation events in urban Leipzig (Germany)", University of Birmingham eData Repository [data set], https://doi.org/10.25500/edata.bham.00001073, 2024.

He, X.-C., Tham, Y. J., Dada, L., et al.: Role of iodine oxoacids in atmospheric aerosol nucleation, Science, 371, 589–595, https://doi.org/10.1126/science.abe0298, 2021.

Hirsikko, A., Nieminen, T., Gagné, S., Lehtipalo, K., Manninen, H. E., Ehn, M., Hõrrak, U., Kerminen, V.-M., Laakso, L., McMurry, P. H., Mirme, A., Mirme, S., Petäjä, T., Tammet, H., Vakkari, V., Vana, M., and Kulmala, M.: Atmospheric ions and nucleation: a review of observations, Atmos. Chem. Phys., 11, 767–798, https://doi.org/10.5194/acp-11-767-2011, 2011.

Hoppel, W. A.: Theory of the electrode effect, J. Atmos. Terr. Phys., 29, 709–721, https://doi.org/10.1016/0021-9169(67)90215-2, 1967.

Hõrrak, U.: Statistical results of air ions and aerosol measurements on the island of Vilsandi in the summer of 1984, Acta Comm. Univ. Tartu, 755, 47–57, 1987.

Hõrrak, U., Salm, J., and Tammet, H.: Diurnal variation in the concentration of air ions of different mobility classes in a rural area, J. Geophys. Res.-Atmos., 108, 4653, https://doi.org/10.1029/2002JD003240, 2003.

Hyttinen, N., Kupiainen-Määttä, O., Rissanen, M. P., Muuronen, M., Ehn, M., and Kurtén, T.: Modeling the Charging of Highly Oxidized Cyclohexene Ozonolysis Products Using Nitrate-Based Chemical Ionization, J. Phys. Chem. A, 119, 6339–6345, https://doi.org/10.1021/acs.jpca.5b01818, 2015.

Jayaratne, E. R., Ling, X., and Morawska, L.: Ions in motor vehicle exhaust and their dispersion near busy roads, Atmos. Environ., 44, 3644–3650, https://doi.org/10.1016/j.atmosenv.2010.06.043, 2010.

Jayaratne, E. R., Ling, X., and Morawska, L.: Corona ions from high-voltage power lines: Nature of emission and dispersion, J. Electrostat., 69, 228–235, https://doi.org/10.1016/j.elstat.2011.03.014, 2011.

Jayaratne, E. R., Ling, X., and Morawska, L.: Observation of ions and particles near busy roads using a neutral cluster and air ion spectrometer (NAIS), Atmos. Environ., 84, 198–203, https://doi.org/10.1016/j.atmosenv.2013.11.045, 2014.

Kelly, F. J. and Fussell, J. C.: Air pollution and public health: emerging hazards and improved understanding of risk, Environ. Geochem. Hlth., 37, 631–649, https://doi.org/10.1007/s10653-015-9720-1, 2015.

Kerminen, V. M., Chen, X., Vakkari, V., Petäjä, T., Kulmala, M., and Bianchi, F.: Atmospheric new particle formation and growth: Review of field observations, Environ. Res. Lett., 13, 103003, https://doi.org/10.1088/1748-9326/aadf3c, 2018.

Kirkby, J., Curtius, J., Almeida, J., Dunne, E., Duplissy, J., Ehrhart, S., Franchin, A., Gagné, S., Ickes, L., Kürten, A., Kupc, A., Metzger, A., Riccobono, F., Rondo, L., Schobesberger, S., Tsagkogeorgas, G., Wimmer, D., Amorim, A., Bianchi, F., Breitenlechner, M., David, A., Dommen, J., Downard, A., Ehn, M., Flagan, R. C., Haider, S., Hansel, A., Hauser, D., Jud, W., Junninen, H., Kreissl, F., Kvashin, A., Laaksonen, A., Lehtipalo, K., Lima, J., Lovejoy, E. R., Makhmutov, V., Mathot, S., Mikkilä, J., Minginette, P., Mogo, S., Nieminen, T., Onnela, A., Pereira, P., Petäjä, T., Schnitzhofer, R., Seinfeld, J. H., Sipilä, M., Stozhkov, Y., Stratmann, F., Tomé, A., Vanhanen, J., Viisanen, Y., Vrtala, A., Wagner, P. E., Walther, H., Weingartner, E., Wex, H., Winkler, P. M., Carslaw, K. S., Worsnop, D. R., Baltensperger, U., and Kulmala, M.: Role of sulphuric acid, ammonia and galactic cosmic rays in atmospheric aerosol nucleation, Nature, 476, 429–433, https://doi.org/10.1038/nature10343, 2011.

Kirkby, J., Amorim, A., Baltensperger, U., Carslaw, K. S., Christoudias, T., Curtius, J., Donahue, N. M., Haddad, I. E., Flagan, R. C., Gordon, H., Hansel, A., Harder, H., Junninen, H., Kulmala, M., Kürten, A., Laaksonen, A., Lehtipalo, K., Lelieveld, J., Möhler, O., Riipinen, I., Stratmann, F., Tomé, A., Virtanen, A., Volkamer, R., Winkler, P. M., and Worsnop, D. R.: Atmospheric new particle formation from the CERN CLOUD experiment, Nat. Geosci., 16, 948–957, https://doi.org/10.1038/s41561-023-01305-0, 2023.

Ku, B. K. and de la Mora, J. F.: Relation between Electrical Mobility, Mass, and Size for Nanodrops 1–6.5 nm in Diameter in Air, Aerosol Sci. Tech., 43, 241–249, https://doi.org/10.1080/02786820802590510, 2009.

Kulmala, M., Riipinen, I., Nieminen, T., Hulkkonen, M., Sogacheva, L., Manninen, H. E., Paasonen, P., Petäjä, T., Dal Maso, M., Aalto, P. P., Viljanen, A., Usoskin, I., Vainio, R., Mirme, S., Mirme, A., Minikin, A., Petzold, A., Hõrrak, U., Plaß-Dülmer, C., Birmili, W., and Kerminen, V.-M.: Atmospheric data over a solar cycle: no connection between galactic cosmic rays and new particle formation, Atmos. Chem. Phys., 10, 1885–1898, https://doi.org/10.5194/acp-10-1885-2010, 2010.

Kulmala, M., Petäjä, T., Nieminen, T., Sipilä, M., Manninen, H. E., Lehtipalo, K., Dal Maso, M., Aalto, P. P., Junninen, H., Paasonen, P., Riipinen, I., Lehtinen, K. E. J., Laaksonen, A. and Kerminen, V.-M.: Measurement of the nucleation of atmospheric aerosol particles, Nat. Protoc., 7, 1651–1667, https://doi.org/10.1038/nprot.2012.091, 2012.

Kürten, A., Rondo, L., Ehrhart, S., and Curtius, J.: Calibration of a Chemical Ionization Mass Spectrometer for the Measurement of Gaseous Sulfuric Acid, J. Phys. Chem. A, 116, 6375–6386, https://doi.org/10.1021/jp212123n, 2012.

Lee, S. H., Gordon, H., Yu, H., Lehtipalo, K., Haley, R., Li, Y., and Zhang, R.: New Particle Formation in the Atmosphere: From Molecular Clusters to Global Climate, J. Geophys. Res.-Atmos., 124, 7098–7146, https://doi.org/10.1029/2018JD029356, 2019.

Mahfouz, N. G. A. and Donahue, N. M.: Technical note: The enhancement limit of coagulation scavenging of small charged particles, Atmos. Chem. Phys., 21, 3827–3832, https://doi.org/10.5194/acp-21-3827-2021, 2021.

Manninen, H. E., Nieminen, T., Asmi, E., Gagné, S., Häkkinen, S., Lehtipalo, K., Aalto, P., Vana, M., Mirme, A., Mirme, S., Hõrrak, U., Plass-Dülmer, C., Stange, G., Kiss, G., Hoffer, A., Törő, N., Moerman, M., Henzing, B., de Leeuw, G., Brinkenberg, M., Kouvarakis, G. N., Bougiatioti, A., Mihalopoulos, N., O'Dowd, C., Ceburnis, D., Arneth, A., Svenningsson, B., Swietlicki, E., Tarozzi, L., Decesari, S., Facchini, M. C., Birmili, W., Sonntag, A., Wiedensohler, A., Boulon, J., Sellegri, K., Laj, P., Gysel, M., Bukowiecki, N., Weingartner, E., Wehrle, G., Laaksonen, A., Hamed, A., Joutsensaari, J., Petäjä, T., Kerminen, V.-M., and Kulmala, M.: EUCAARI ion spectrometer measurements at 12 European sites – analysis of new particle formation events, Atmos. Chem. Phys., 10, 7907–7927, https://doi.org/10.5194/acp-10-7907-2010, 2010.

Mercer, J. and Wilson, B.: Daily Variation of Cosmic Rays, Nature, 208, 477–479, https://doi.org/10.1038/208477a0, 1965.

Mikhailov, A.: Turbo, An Improved Rainbow Colormap for Visualization, Google Research Blog, https://blog.research.google/2019/08/turbo-improved-rainbow-colormap-for.html (last access: 4 December 2023), 2019.

Mirme, S. and Mirme, A.: The mathematical principles and design of the NAIS – a spectrometer for the measurement of cluster ion and nanometer aerosol size distributions, Atmos. Meas. Tech., 6, 1061–1071, https://doi.org/10.5194/amt-6-1061-2013, 2013.

Pushpawela, B., Jayaratne, R., and Morawska, L.: Temporal distribution and other characteristics of new particle formation events in an urban environment, Environ. Pollut., 233, 552–560, https://doi.org/10.1016/j.envpol.2017.10.102, 2018.

Quaas, J., Ming, Y., Menon, S., Takemura, T., Wang, M., Penner, J. E., Gettelman, A., Lohmann, U., Bellouin, N., Boucher, O., Sayer, A. M., Thomas, G. E., McComiskey, A., Feingold, G., Hoose, C., Kristjánsson, J. E., Liu, X., Balkanski, Y., Donner, L. J., Ginoux, P. A., Stier, P., Grandey, B., Feichter, J., Sednev, I., Bauer, S. E., Koch, D., Grainger, R. G., Kirkevåg, A., Iversen, T., Seland, Ø., Easter, R., Ghan, S. J., Rasch, P. J., Morrison, H., Lamarque, J.-F., Iacono, M. J., Kinne, S., and Schulz, M.: Aerosol indirect effects – general circulation model intercomparison and evaluation with satellite data, Atmos. Chem. Phys., 9, 8697–8717, https://doi.org/10.5194/acp-9-8697-2009, 2009.

Rose, C., Foucart, B., Picard, D., Colomb, A., Metzger, J.-M., Tulet, P., and Sellegri, K.: New particle formation in the volcanic eruption plume of the Piton de la Fournaise: specific features from a long-term dataset, Atmos. Chem. Phys., 19, 13243–13265, https://doi.org/10.5194/acp-19-13243-2019, 2019.

Seinfeld, J. H. and Pandis, S. N.: Atmospheric Chemistry and Physics: From Air Pollution to Climate Change, John Wiley & Sons, Hoboken, ISBN: 978-1-118-94740-1 2016.

Simon, M., Dada, L., Heinritzi, M., Scholz, W., Stolzenburg, D., Fischer, L., Wagner, A. C., Kürten, A., Rörup, B., He, X.-C., Almeida, J., Baalbaki, R., Baccarini, A., Bauer, P. S., Beck, L., Bergen, A., Bianchi, F., Bräkling, S., Brilke, S., Caudillo, L., Chen, D., Chu, B., Dias, A., Draper, D. C., Duplissy, J., El-Haddad, I., Finkenzeller, H., Frege, C., Gonzalez-Carracedo, L., Gordon, H., Granzin, M., Hakala, J., Hofbauer, V., Hoyle, C. R., Kim, C., Kong, W., Lamkaddam, H., Lee, C. P., Lehtipalo, K., Leiminger, M., Mai, H., Manninen, H. E., Marie, G., Marten, R., Mentler, B., Molteni, U., Nichman, L., Nie, W., Ojdanic, A., Onnela, A., Partoll, E., Petäjä, T., Pfeifer, J., Philippov, M., Quéléver, L. L. J., Ranjithkumar, A., Rissanen, M. P.,

Schallhart, S., Schobesberger, S., Schuchmann, S., Shen, J., Sipilä, M., Steiner, G., Stozhkov, Y., Tauber, C., Tham, Y. J., Tomé, A. R., Vazquez-Pufleau, M., Vogel, A. L., Wagner, R., Wang, M., Wang, D. S., Wang, Y., Weber, S. K., Wu, Y., Xiao, M., Yan, C., Ye, P., Ye, Q., Zauner-Wieczorek, M., Zhou, X., Baltensperger, U., Dommen, J., Flagan, R. C., Hansel, A., Kulmala, M., Volkamer, R., Winkler, P. M., Worsnop, D. R., Donahue, N. M., Kirkby, J., and Curtius, J.: Molecular understanding of new-particle formation from $\alpha$-pinene between $-50$ and $+25$ °C, Atmos. Chem. Phys., 20, 9183–9207, https://doi.org/10.5194/acp-20-9183-2020, 2020.

Spracklen, D. V., Carslaw, K. S., Merikanto, J., Mann, G. W., Reddington, C. L., Pickering, S., Ogren, J. A., Andrews, E., Baltensperger, U., Weingartner, E., Boy, M., Kulmala, M., Laakso, L., Lihavainen, H., Kivekäs, N., Komppula, M., Mihalopoulos, N., Kouvarakis, G., Jennings, S. G., O'Dowd, C., Birmili, W., Wiedensohler, A., Weller, R., Gras, J., Laj, P., Sellegri, K., Bonn, B., Krejci, R., Laaksonen, A., Hamed, A., Minikin, A., Harrison, R. M., Talbot, R., and Sun, J.: Explaining global surface aerosol number concentrations in terms of primary emissions and particle formation, Atmos. Chem. Phys., 10, 4775–4793, https://doi.org/10.5194/acp-10-4775-2010, 2010.

Suni, T., Kulmala, M., Hirsikko, A., Bergman, T., Laakso, L., Aalto, P. P., Leuning, R., Cleugh, H., Zegelin, S., Hughes, D., van Gorsel, E., Kitchen, M., Vana, M., Hõrrak, U., Mirme, S., Mirme, A., Sevanto, S., Twining, J., and Tadros, C.: Formation and characteristics of ions and charged aerosol particles in a native Australian Eucalypt forest, Atmos. Chem. Phys., 8, 129–139, https://doi.org/10.5194/acp-8-129-2008, 2008.

Svensmark, H., Enghoff, M. B., Shaviv, N. J., and Svensmark, J.: Increased ionization supports growth of aerosols into cloud condensation nuclei, Nat. Commun., 8, 2199, https://doi.org/10.1038/s41467-017-02082-2, 2017.

Tammet, H.: Continuous scanning of the mobility and size distribution of charged clusters and nanometer particles in atmospheric air and the Balanced Scanning Mobility Analyzer BSMA, Atmos. Res., 82, 523–535, https://doi.org/10.1016/j.atmosres.2006.02.009, 2006.

Tammet, H., Hõrrak, U., Laakso, L., and Kulmala, M.: Factors of air ion balance in a coniferous forest according to measurements in Hyytiälä, Finland, Atmos. Chem. Phys., 6, 3377–3390, https://doi.org/10.5194/acp-6-3377-2006, 2006.

Tammet, H., Hõrrak, U., and Kulmala, M.: Negatively charged nanoparticles produced by splashing of water, Atmos. Chem. Phys., 9, 357–367, https://doi.org/10.5194/acp-9-357-2009, 2009.

Tammet, H., Komsaare, K., and Hõrrak, U.: Intermediate ions in the atmosphere, Atmos. Res., 135–136, 263–273, https://doi.org/10.1016/j.atmosres.2012.09.009, 2014.

Thomas, A. E., Bauer, P. S., Dam, M., Perraud, V., Wingen, L. M., and Smith, J. N.: Automotive braking is a source of highly charged aerosol particles, P. Natl. Acad. Sci. USA, 121, e2313897121, https://doi.org/10.1073/pnas.2313897121, 2024.

Tian, M., Wang, H., Chen, Y., Yang, F., Zhang, X., Zou, Q., Zhang, R., Ma, Y., and He, K.: Characteristics of aerosol pollution during heavy haze events in Suzhou, China, Atmos. Chem. Phys., 16, 7357–7371, https://doi.org/10.5194/acp-16-7357-2016, 2016.

Uusitalo, H., Kontkanen, J., Ylivinkka, I., Ezhova, E., Demakova, A., Arshinov, M., Belan, B. D., Davydov, D., Ma, N., Petäjä, T., Wiedensohler, A., Kulmala, M., and Nieminen, T.: Occurrence of new particle formation events in Siberian and Finnish boreal forest, Atmos. Chem. Phys. Discuss. [preprint], https://doi.org/10.5194/acp-2021-530, 2021.

Vana, M., Ehn, M., Petäjä, T., Vuollekoski, H., Aalto, P., de Leeuw, G., Ceburnis, D., O'Dowd, C. D., and Kulmala, M.: Characteristic features of air ions at Mace Head on the west coast of Ireland, Atmos. Res., 90, 278–286, https://doi.org/10.1016/j.atmosres.2008.04.007, 2008.

Wang, J. and Li, S.: Changes in negative air ions concentration under different light intensities and development of a model to relate light intensity to directional change, J. Environ. Manage., 90, 2746–2754, 2009.

Wang, Y., Zhuang, G., Tang, A., Yuan, H., Sun, Y., Chen, S., and Zheng, A.: The ion chemistry and the source of PM2.5 aerosol in Beijing, Atmos. Environ., 39, 3771–3784, https://doi.org/10.1016/j.atmosenv.2005.03.013, 2005.

Wiedensohler, A., Birmili, W., Nowak, A., Sonntag, A., Weinhold, K., Merkel, M., Wehner, B., Tuch, T., Pfeifer, S., Fiebig, M., Fjäraa, A. M., Asmi, E., Sellegri, K., Depuy, R., Venzac, H., Villani, P., Laj, P., Aalto, P., Ogren, J. A., Swietlicki, E., Williams, P., Roldin, P., Quincey, P., Hüglin, C., Fierz-Schmidhauser, R., Gysel, M., Weingartner, E., Riccobono, F., Santos, S., Grüning, C., Faloon, K., Beddows, D., Harrison, R., Monahan, C., Jennings, S. G., O'Dowd, C. D., Marinoni, A., Horn, H.-G., Keck, L., Jiang, J., Scheckman, J., McMurry, P. H., Deng, Z., Zhao, C. S., Moerman, M., Henzing, B., de Leeuw, G., Löschau, G., and Bastian, S.: Mobility particle size spectrometers: harmonization of technical standards and data structure to facilitate high quality long-term observations of atmospheric particle number size distributions, Atmos. Meas. Tech., 5, 657–685, https://doi.org/10.5194/amt-5-657-2012, 2012.

Yan, C., Dada, L., Rose, C., Jokinen, T., Nie, W., Schobesberger, S., Junninen, H., Lehtipalo, K., Sarnela, N., Makkonen, U., Garmash, O., Wang, Y., Zha, Q., Paasonen, P., Bianchi, F., Sipilä, M., Ehn, M., Petäjä, T., Kerminen, V.-M., Worsnop, D. R., and Kulmala, M.: The role of $H_2SO_4$-$NH_3$ anion clusters in ion-induced aerosol nucleation mechanisms in the boreal forest, Atmos. Chem. Phys., 18, 13231–13243, https://doi.org/10.5194/acp-18-13231-2018, 2018.

Yao, L., Garmash, O., Bianchi, F., Zheng, J., Yan, C., Kontkanen, J., Junninen, H., Mazon, S. B., Ehn, M., Paasonen, P., Sipilä, M., Wang, M., Wang, X., Xiao, S., Chen, H., Lu, Y., Zhang, B., Wang, D., Fu, Q., Geng, F., Li, L., Wang, H., Qiao, L., Yang, X., Chen, J., Kerminen, V. M., Petäjä, T., Worsnop, D. R., Kulmala, M., and Wang, L.: Atmospheric new particle formation from sulfuric acid and amines in a Chinese megacity, Science, 361, 278–281, https://doi.org/10.1126/science.aao4839, 2018.

Zauner-Wieczorek, M., Curtius, J., and Kürten, A.: The ion–ion recombination coefficient $a$: comparison of temperature- and pressure-dependent parameterisations for the troposphere and stratosphere, Atmos. Chem. Phys., 22, 12443–12465, https://doi.org/10.5194/acp-22-12443-2022, 2022.

Zhang, K., Feichter, J., Kazil, J., Wan, H., Zhuo, W., Griffiths, A. D., Sartorius, H., Zahorowski, W., Ramonet, M., Schmidt, M., Yver, C., Neubert, R. E. M., and Brunke, E.-G.: Radon activity in the lower troposphere and its impact on ionization rate: a global estimate using different radon emissions, Atmos. Chem. Phys., 11, 7817–7838, https://doi.org/10.5194/acp-11-7817-2011, 2011.